Bone 120 (2019) 156–165

Contents lists available at ScienceDirect

Bone

journal homepage: www.elsevier.com/locate/bone

Full Length Article

SF-deferoxamine, a bone-seeking angiogenic drug, prevents bone loss in estrogen-deficient mice

Changjun Guo[a,b,1], Kai Yang[a,1], Yufei Yan[a,1], Dongming Yan[d], Yifan Cheng[d], Xueming Yan[a], Niandong Qian[a], Qi Zhou[a], Bo Chen[a], Min Jiang[a], Hanbing Zhou[a], Changwei Li[a], Fei Wang[a], Jin Qi[a,*], Xiangyang Xu[b,c,**], Lianfu Deng[a,*]

[a] Shanghai Key Laboratory for Prevention and Treatment of Bone and Joint Diseases with Integrated Chinese-Western Medicine, Shanghai Institute of Traumatology and Orthopedics, Ruijin Hospital, Shanghai Jiao Tong University School of Medicine, 197 Ruijin 2nd Road, Shanghai 200025, China
[b] Department of Orthopedics, Rui Jin North Hospital, Shanghai Jiao Tong University School of Medicine, 999 Xiwang Road, Shanghai 201801, China
[c] Department of Orthopedics, Ruijin Hospital, Shanghai Jiao Tong University School of Medicine, 197 Ruijin 2nd Road, Shanghai 200025, China
[d] National Shanghai Center for New Drug Safety Evaluation and Research, 199 Guoshoujing Road, China (Shanghai) Pilot Free Trade Zone, Shanghai 201203, China

ARTICLE INFO

Keywords:
Deferoxamine
Osteoporosis
Bone-seeking
Angiogenesis
HIF

ABSTRACT

Deferoxamine (DFO) possesses a good chelating capability and is therefore used for the clinical treatment of ion deposition diseases. Increasing evidence shows that DFO can inhibit the activity of proline hydroxylase (PHD) by chelating iron, resulting in hypoxia-induced factor (HIF) signaling activation and angiogenesis promotion. However, clinical evidence indicates that a high concentration of DFO could be biotoxic due to its enrichment in related organs. Thus, we established a new compound by conjugating DFO with the bone-seeking agent iminodiacetic acid (IDA); the new agent is called SF-DFO, and we verified its promotion of HIF activation and tube formation in vivo. After confirming the bone-seeking property of SF-DFO in the femur and vertebra of both male and female mice and comparing it to that of DFO, we analyzed the protective effect of DFO and SF-DFO in an ovariectomized (OVX) mouse model. The serum CTX-I level revealed no influence of DFO and SF-DFO on osteoclast activity, but the blood vessels and osteoblasts in the metaphysis were more abundant after SF-DFO treatment, which resulted in a greater protective effect against trabecular bone loss compared to the DFO group. Additionally, the cortical parameters and bone strength performance were identical between the DFO and SF-DFO groups. However, the diffuse inflammatory response in the liver and spleen that occurred after DFO injection was not observed in the SF-DFO group. Thus, with reduced biotoxicity and an equivalent bone-seeking capability, SF-DFO may be a better choice for the prevention of vascular degradation-induced osteoporosis.

1. Introduction

Osteoporosis is the most common metabolic bone disease, and the main pathological features that increase with age are progressive bone loss, bone microstructure degeneration, increased bone fragility and proneness to fracture [1]. Estrogen deficiency is the most common cause [2], followed by a decrease in the number of capillaries in the bone marrow and therefore oxygen perfusion [3–5].

HIFs (hypoxia-inducible factors) are the most direct or unique regulatory factors that have been discovered in tissue cells in the hypoxic state, and there are three subtypes (HIF-1α, HIF-2α, HIF-3α) [6]. Under normal oxygen conditions, the proline residues of HIFα are hydroxylated by prolyl-4-hydroxylase domains (PHDs) with Fe^{2+}. Then, the hydroxylated HIFα is recognized by pVHL (Von Hippel-Lindau) and is eventually degraded [7]. When the cell suffers from a hypoxic state or a lack of Fe^{2+}, which results in a decrease or inactivation of PHD activity, or when the expression of pVHL is reduced or even absent, HIFα will accumulate and move into the nucleus, in turn activating the transcription of numerous HIF target genes involved in angiogenesis, glucose and energy metabolism, erythropoiesis, cell proliferation, apoptosis and oxygen response [8–10].

In our previous research, conditional pVHL knockout mice with

* Corresponding authors.
** Correspondence to: X. Xu, Department of Orthopedics, Rui Jin Hospital, Shanghai Jiao Tong University School of Medicine, 197 Ruijin 2nd Road, Shanghai 200025, China.
E-mail addresses: jinjin838@hotmail.com (J. Qi), xu664531@hotmail.com (X. Xu), lf_deng@126.com (L. Deng).
[1] These authors contributed equally to this work.

https://doi.org/10.1016/j.bone.2018.10.025
Received 30 May 2018; Received in revised form 28 October 2018; Accepted 29 October 2018
Available online 30 October 2018

osteocalcin-positive osteoblasts demonstrated an marked bone formation capacity throughout life, which resulted from the enhanced vascular network [11]. Clearly, enhancing HIFα expression in the bone microenvironment is beneficial for promoting angiogenesis in bone tissue, establishing a new blood supply, accelerating bone formation, and even attenuating OVX-induced progressive bone loss [12]. To date, a number of HIFα activators that target PHDs have been identified from natural small-molecule compounds and their derivatives [13]. Among them, deferoxamine (DFO), a Fe^{2+} chelator, has long been used in curing iron overload patients with thalassemia major [14,15]. By promoting HIF-1α accumulation and vascular endothelial growth factor (VEGF) expression, DFO can improve vascularity and accelerate bone regeneration in bone fracture repair [16,17]. However, despite the clear advantages of DFO, numerous significant drug-related systemic toxicities have been reported in the literature, including toxicities in the cardiovascular, respiratory, gastrointestinal, cutaneous, and nervous systems [18]; in addition, DFO is associated with a propensity for bone dysplasia [19] and high-frequency sensorineural hearing loss [20–22].

It has been reported that by conjugating them with a bone-seeking agent, including bisphosphonate or tetracycline, bone-preservative drugs could be specifically delivered to bone tissue, thereby reducing side effects due to nonspecific tissue interactions [23,24]. Iminodiacetic acid (IDA, $NH(CH_2COOH)_2$), a calcium chelator that has a high affinity for calcium and is used in the clinical treatment of patients with heavy metal poisoning [25], has been demonstrated to concentrate 17β-estradiol in bone tissue by combining with calcium [26].

In this study, we covalently modified DFO by conjugating it with IDA (Fig. 1, SF-DFO, patent CN 106008256A) and demonstrated that SF-DFO retains its functions of activating HIF-1α and promoting tube formation in vivo. A tissue distribution assay validated that compared to DFO, after i.v. injection, SF-DFO accumulated in bone tissue and remained at a steady concentration there for 24 h. Furthermore, SF-DFO had a marked preventative against OVX-induced bone loss, with fewer organ biotoxicities compared to DFO.

2. Materials and methods

2.1. SF-deferoxamine synthesis

The mixture of compound 2 (5.00 g), *p*-toluene sulfonic acid (7.76 g), benzyl alcohol (50 ml) and toluene (150 ml) was heated to 150 °C. Water was removed through azeotropic distillation for 10 h and cooled to room temperature. A large amount of solid was gradually precipitated for 2 h. The solid was filtrated and dried under vacuum at 50 °C. The white solid was dissolved in water (100 ml) and dichloromethane (100 ml) was added. The pH was adjusted to 7.0 with diluted $NaHCO_3$ (1 M) under ice-bath. The organic phase was washed with brine, dried over anhydrous magnesium sulfate, filtered and concentrated to give compound 3 (9.92 g) as a pale yellow oil.

The mixture of compound 3 (3.00 g), succinic anhydride (1.10 g), triethylamine (1.94 g), methyl tertiary ether (20 ml) was heated to 50 °C for 3 h and cooled to room temperature. Then water (20 ml) was added. The pH was adjusted to 3.0 with dilute hydrochloric acid under ice-bath. The organic layer was separated and washed with saturated brine, dried over anhydrous magnesium sulfate and filtered. The resulting organic phase was concentrated to give compound 4 (3.58 g) as a pale yellow oil.

0.30 g of compound 5 (Desferrioxamine mesylate DFO), *N*,*N*-dimethylformamide (DMF) (15 ml), *N*-methyl morpholine (NMM, 0.231 g) was mixed at room temperature. PyBoP and the solution of compound 4 in DMF (5 ml) was added and stirred at room temperature for 24 h. Then the solid was filtrated and then dried under vacuum at 40 °C to give compound 6 (0.30 g).

Compound 6 (0.30 g), Pd/C (20%, 0.05 g), *N*,*N*-dimethylformamide (20 ml) was added to a hydrogenation reaction vessel under 11 atm H_2 and reacted at 50 °C for 6 h. The liquid was separated by filtration. White solid was precipitated after the addition of ethanol to the concentrated DMF. The solid was filtrated and dried under vacuum at 30 °C for 6 h to give SF-DFO (0.24 g).

Element analysis $C_{33}H_{57}N_7O_{14}$, theoretic value (%): C 51.09, H 7.41, N 12.64; measured value (%): C 51.05, H 7.44, N 12.69. ^{1}H NMR (500 MHz, DMSO-d_6) δ (ppm): 9.55 (m, 2H, $-CH_2COO-$), 6.69-7.71 (m, 3H, $-NH-$), 3.95-4.15 (m, 4H, $-CH_2-$), 3.44-3.47 (m, 6H, $-CH_2-$), 2.98-3.03 (m, 6H, $-CH_2-$), 2.51-2.59 (m, 4H, $-CH_2-$), 2.5 (m, 2H, $-CH_2-$), 2.45-2.49 (m, 4H, $-CH_2-$), 1.97 (m, 2H, $-CH_2-$), 1.49-1.54 (m, 3H, $-OH$), 1.47 (m, 3H, $-CH_2-$), 1.35-1.42 (m, 12H, $-CH_2-$), 1.2-1.26 (m, 6H, $-CH_2-$), MS (EI) *m/z*: 775.7, as shown in Supplementary Fig. 1.

The chemical compounds used in SF-DFO synthesis, including iminodiacetic acid, benzyl alcohol, toluene, *p*-toluenesulfonic acid, succinic anhydride, triethylamine, methyl tertiary ether and desferrioxamine mesylate DFO, were all purchased from SIGMA-ALDRICH (USA).

2.2. Osteoblast isolation and treatments

Primary osteoblasts were isolated from the calvarias of newborn C57/B6 mice by serial round type I collagenase digestion and cultured in 10% FBS containing alpha-MEM with penicillin and streptomycin as described previously [27]. The fourth-generation osteoblasts were used for the following experiments. HUVECs were cultured in 10% FBS containing DMEM with penicillin and streptomycin. Due to the hydrophobic properties of SF-DFO, DFO and SF-DFO were both dissolved in DMSO and subjected to cellular and animal treatment.

2.3. Western blot

After 100 μM and 200 μM DFO and SF-DFO treatment for 24 h, primary osteoblasts seeded in 12-well plates were directly lysed with Laemmli buffer. Proteins were separated in 10% SDS–PAGE and transferred to nitrocellulose membranes. After blocking with 5% milk in TBS-T buffer, proteins were detected using various antibodies against HIF1A (#A7684, ABclonal, China) and α-tubulin (#ab7291, Abcam, USA) at 4 °C overnight. The membranes were incubated with peroxidase-conjugated secondary antibodies (1:5000, Jackson) for 1 h at 37 °C before detection using the ECL system (EMD Millipore).

2.4. RT-PCR

The fourth-generation primary osteoblasts were seeded in 12-well plates. After treatments with various concentrations of DFO and SF-DFO, total RNA was isolated from osteoblasts using Trizol reagent (Invitrogen) according to the manufacturer's instructions. Next, cDNA was synthesized from 2 μg of total RNA using reverse transcriptase (TakaRa, Shiga, Japan). qRT-PCR was performed to amplify the cDNA using the SYBR Premix Ex Tag kit (TaKaRa) on an ABI 7500 Sequencing Detection System (Applied Biosystems, USA) in three triplicated wells. The following cycling conditions were used: 40 cycles of denaturation at 95 °C for 5 s and amplification at 60 °C for 40 s. β-Actin was used as the housekeeping gene, and all reactions were run in triplicate. The mouse primer sequences for VEGF (Accession Numbers: NM_001025250.3), HO-1 (Accession Numbers: NM_010442.2) and β-actin (Accession Numbers: NM_007393) are shown in Supplementary Table 1.

2.5. Dual luciferase assay

Mouse primary osteoblasts were seeded into 24-well plates and were co-transfected with PGL3-basic-HRE-luciferase and Renilla luciferase expressing vectors. After one day, cells were treated with 100 μM or 200 μM DFO and SF-DFO for 24 h. Then, Firefly and Renilla luciferase activities were measured using a Dual Luciferase Assay kit (Promega, USA). Firefly luciferase activity was normalized to Renilla luciferase

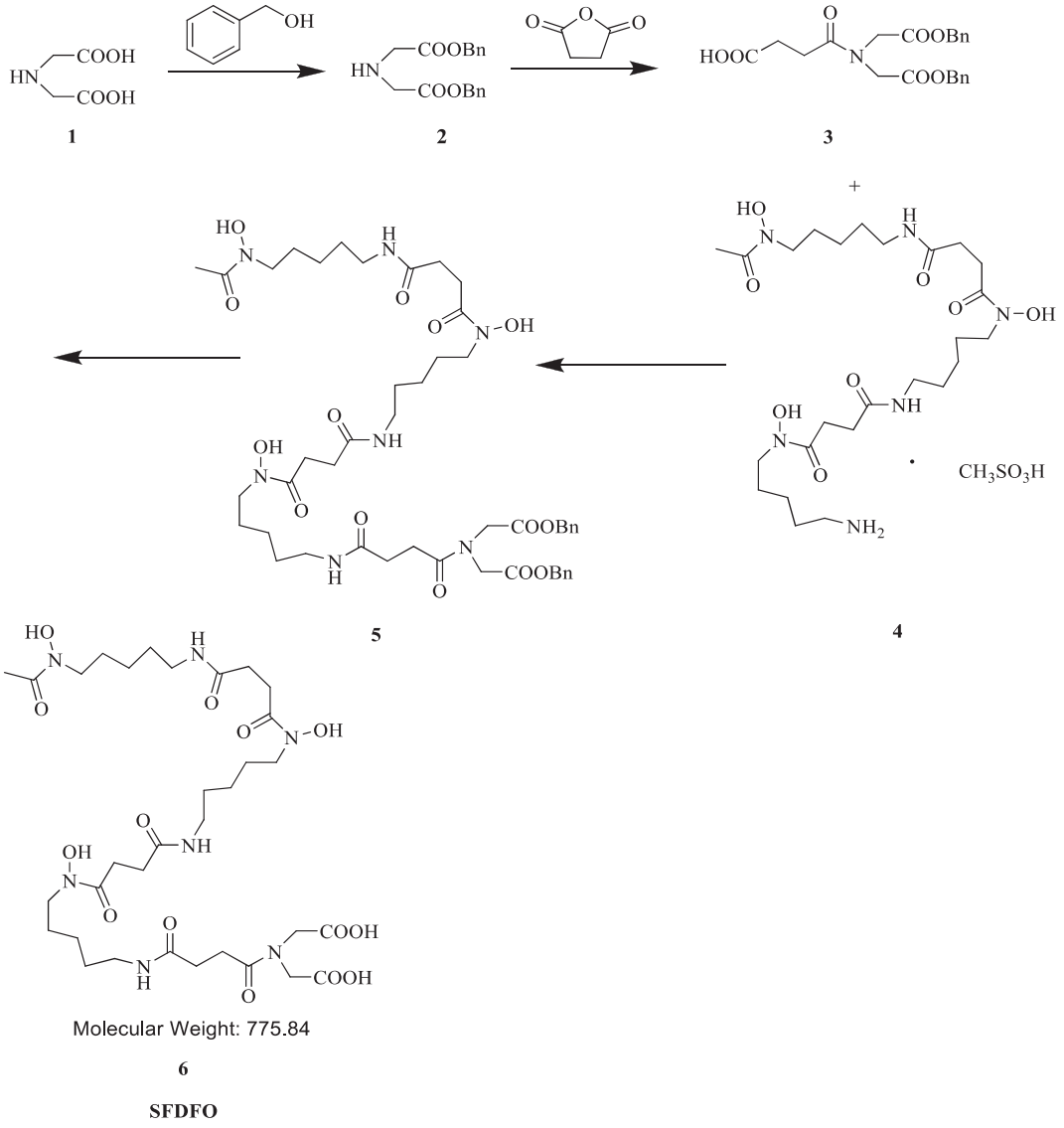

Fig. 1. The route of synthesizing SF-deferoxamine. According to the synthetic flow in patent CN 106008256A, iminodiacetic acid was protected by benzyl alcohol to prepare compound 2, which was condensed with succinic anhydride to afford the side chain-compound 3. Then, compound 4, desferrioxamine mesylate, was reacted with compound 3, and, with the deprotection of compound 5, the target compound SF-DFO was finally prepared.

activity. Experiments were performed in triplicate. Original data were analyzed and exported from GraphPad Prism software.

2.6. Tube formation assay

HUVECs were purchased from Cell Bank, Shanghai Institutes for Biological Sciences, Chinese Academy of Sciences, Shanghai. To assess the angiogenesis promoting ability of DFO and SF-DFO, 5×10^4 HUVECs were gently mixed with 0.1 ml growth factor-reduced Matrigel (BD Biosciences, US) and seeded in a 24-well plate. After 24 h, cells were treated with 200 μM DFO and SF-DFO for another 12 h to induce tube formation. The cells were then fixed with 4% paraformaldehyde. After Texas Red-X Phalloidin and DAPI (Beyotime Biotechnology, Shanghai) staining, complete tube structures were visualized on an LSM 810 confocal microscope with a 4× objective (ZEISS) using the *Z*-axis topologic reconstruction method. All the images were analyzed in ImageJ software (version 1.51w with 64-bit Java Platform; NIH). The average value of the complete tube parameters was calculated using the Angiogenesis Analyzer plugin (https://imagej.nih.gov/ij/) based on five random fields in each image.

2.7. Animal experiments

C57BL/6 mice were all purchased from the Shanghai SLAC Laboratory (Shanghai, China). All the procedures involving mice experiments were approved by the Shanghai Jiaotong University Animal Care and Use Committee in direct accordance with the Ministry of Science and Technology of the People's Republic of China on Animal Care guidelines. Then, 0.25% pentobarbital sodium dissolved in saline was i.p. injected for anesthesia according to the body weight of each mouse.

2.8. Bone tissue distribution

Tissue distribution experiments were all performed in the Center for Drug Safety Evaluation and Research (Shanghai, China) in a double blind manner. According to the minimal requirements for clinical pharmacokinetics, three mice were used in each group of this experiment for statistical analysis. Twenty-four 8-week-old C57BL/6 male and female mice were divided into 4 groups in a completely randomized manner and fasted overnight before the day of administration but

allowed to drink water freely. The next day, 100 μl DFO and SF-DFO solution (containing 1.7857 μmol DFO and SF-DFO) were i.v. injected once, according to the recommended DFO i.v. injection dose [28]. After 0.5, 2, 8, and 24 h, mice were euthanized by CO_2 asphyxiation. A certain amount of muscle-free femurs and vertebrae were weighed, dried and ground to a fine powder, extracted with acetonitrile and subjected to LC-MS/MS validation. Blank mice tissue was used for standard curve preparation. Original data were analyzed and exported from GraphPad Prism software.

2.9. Ovariectomized mouse model

Twenty 8-week-old C57BL/6 female mice were randomly divided into four groups. After anesthesia, five of them were subjected to a sham-operated experiment (as SHAM group), where the rest of them were all subjected to bilateral ovariectomy. After 4 weeks, the OVX mice were separated into three groups and were individually i.p. injected with vehicle (as OVX group), 40 mg/kg DFO (as DFO group) and 55.4 mg/kg SF-DFO (as SF-DFO group) every day for another 4 weeks, according to the recommended DFO i.p. injection dose [29]. Five mice were housed in one cage and maintained under a strict 12-h light, 12-h dark cycle at 22 °C with standard mice food pellets and had free access to tap water. Mouse weight was recorded every 7 days. At last, mice were euthanized by CO_2 asphyxiation, and the serum, kidney, spleen, liver and femurs were all collected and subjected to subsequent analysis.

2.10. Micro-computed tomography

Micro-CT analysis was performed on the left femur of each mouse. After fixation with 4% paraformaldehyde, the femurs were scanned on a Skyscan 1172 (Aartselaar, Belgium) with a 10-μm isotropic voxel size, 50 keV, 500 μA, and 0.7° rotation step, in accordance with the recommendations of the American Society for Bone and Mineral Research (ASBMR) [30]. Regions of interest (ROIs) were defined for trabecular and cortical parameters. The trabecular ROI extended from 1 mm proximally to the end of the distal growth plate over 1 mm toward the diaphysis. The cortical ROI extended from 3 mm proximally to the end of the distal growth plate over 1 mm toward the diaphysis. The resulting two-dimensional images of trabecular and cortical bone in relative cross-sections were shown in grayscale. Trabecular bone parameters were measured including cancellous bone mineral density (Cn-BMD), bone volume/tissue volume (Cn-BV/TV), trabecular thickness (Tb.Th), and trabecular separation (Tb.Sp). Cortical bone parameters were measured including tissue mineral density (TMD), marrow volume (Ma.V), cortical thickness (Ct.Th) and Cortical porosity (Ct.Po).

2.11. Bone histomorphometry

After Micro-computed tomography analysis, the left femurs were both subjected to decalcification and made to paraffin-embedded 10-μm sections for bone histomorphometry analysis. Measurements were done on four sections from different mice in each group and data were presented in accordance with the recommendations of the American Society for Bone and Mineral Research standardized histomorphometry nomenclature [30]. Osteoblast number per bone surface (N.Ob/BS) was measured on H&E-stained sections. Osteoclast number per bone surface (N.Oc/BS) was measured on tartrate-resistant acid phosphatase (TRAP)-stained sections.

2.12. Blood vessels evaluation

Deparaffinized femur sections were incubated with 5% BSA containing anti-α-SMA primary antibody (1:100) (#ab5694, Abcam, USA) at 4 °C overnight. Next day, sections were stained with Alexa Fluor 488-labelled goat anti-rabbit secondary antibody (Invitrogen) at 37 °C for 2 h and counterstained with 4,6-diamidino-2-phenylindole (Beyotime, China) for observation. Images were taken on the metaphysis of each femur using Zeiss 810 laser scanning confocal microscopy system on a Zeiss Axio Observer Z1 inverted microscope, equipped with a Plan-Apochromat 20×, 0.75 NA, differential interference contrast objective and switching reconstruction method. The round or elliptical α-SMA positive area was regard as the blood vessel.

2.13. Histopathology examination and immunohistochemistry

The fixed kidney, spleen and liver were dehydrated and embedded in paraffin. Serial 5-μm sections were prepared for H&E staining and immunohistochemistry.

For immunohistochemistry, endogenous peroxidases were blocked with 1% H_2O_2 in methanol for 15 min and antigen retrieval was performed with microwave boiling in sodium citrate-EDTA buffer for 5 min twice. Then, primary antibody anti-CD45 (1:100) (#ab10558, Abcam, USA) was incubated for overnight at 4 °C. Next day, biotin conjugated secondary antibody (#65–6140, Invitrogen, USA), HRP-conjugated Streptavidin (#434323, Invitrogen, USA) and DAB kit (Boster biological technology Co., China) were used according to the manufacturer's instructions. Nucleus was stained with haematoxylin (Sigma). The 8-bit TIFF images were visualized and exported with a ZEISS Axioskop microscope.

2.14. Three-point bending test

The right femurs from all groups were immediately subjected to a three-point bending test with an Instron 5569 materials mechanical testing system (Instron Inc., MA). Femurs were placed posterior side down between two supports 6 mm apart, and load was applied at the midspan, which made bending occur along the anteroposterior axis. Load-displacement curves were recorded at a crosshead speed of 1 mm/s.

2.15. Statistics

All the original data were analyzed and plotted with GraphPad Prism software (version 6.0c). Statistical analysis was performed with One-way ANOVA. Data are shown as the means ± SD. P values indicate the significant differences.

3. Results

3.1. SF-deferoxamine has an identical hypoxia-inducing effect to deferoxamine

To determine whether the performance of DFO in terms of HIFα pathway activation is altered after modification with IDA, we first analyzed the hypoxia-inducing capability of SF-DFO in primary murine osteoblasts compared to the lead compound of DFO. The results showed that after treatment with 100 μM and 200 μM SF-DFO, the protein level of HIF-1α accumulated, which is similar to the result obtained after treatment with DFO (Fig. 2a, b). Furthermore, the HRE-luciferase reporter system in primary murine osteoblasts also indicated that 200 μM SF-DFO and DFO have comparable capacities in terms of activating HRE-mediated transcription (Fig. 2c). Next, we detected the mRNA level of VEGF, which is downstream of the HIF-1α signaling pathway and plays a pivotal role in promoting angiogenesis. As expected, the mRNA levels of VEGF and heme oxygenase 1 (HO-1) equivalently increased after treatment with DFO and SF-DFO in a dose-dependent manner (Fig. 2d). These results suggest that after combining with IDA, SF-DFO retains the capacity to activate the HIFα signaling pathway.

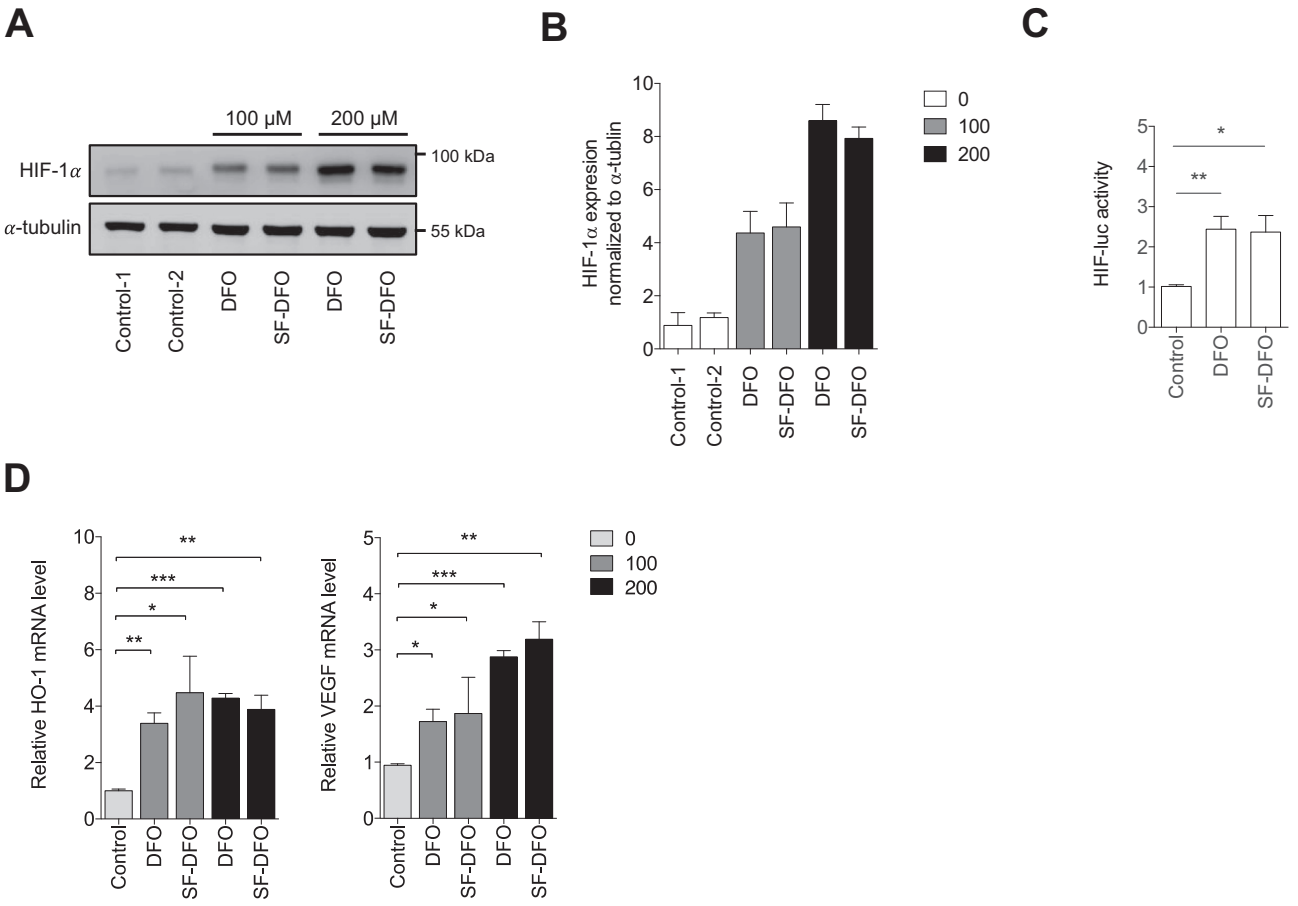

Fig. 2. SF-deferoxamine has an identical hypoxia-inducing effect to deferoxamine. A) The primary osteoblasts were treated with 100 μm and 200 μm DFO or SF-DFO for 24 h, and representative images of HIF-1α protein levels from three independent experiments are shown. Two parallel control samples were used. The uncropped images are shown in Supplementary Fig. 2. B) Gray value analysis of HIF-1α protein against α-tubulin protein in A. C) Primary osteoblasts were cotransfected with PGL3-basci-HRE luciferase reporter and Renilla vectors and treated with 200 μm SF-DFO or DFO for 24 h. HRE-reporter activities from two independent experiments were detected with the dual-luciferase reporter kit. D) Primary osteoblasts were treated with 100 μm and 200 μm SF-DFO or DFO for 24 h, and the VEGF and HO-1 mRNA levels were analyzed. Two independent experiments were performed. One-way ANOVA. Data are represented as the means ± SD. *,$P < 0.05$. **,$P < 0.01$, ***,$P < 0.001$. HRE, hypoxia response element.

3.2. SF-deferoxamine has an identical angiogenesis-promoting effect to deferoxamine

VEGF is responsible for vascular endothelial growth and angiogenesis, and the level of VEGF increases after SF-DFO treatment. Thus, we performed a tube formation assay with cultured human umbilical vein endothelial cells (HUVECs). HUVECs were cultured in growth factor-reduced Matrigel and treated with 200 μM DFO or SF-DFO for 12 h. Then, Texas red-conjugated phalloidin was used to stain the cell structure and tube matrix. Photographs were taken on a confocal microscope with the *Z*-axis topologic reconstruction method. The results showed that the average total length, junction number, mesh area and mesh number of complete tubes all displayed identical levels between the DFO and SF-DFO groups (Fig. 3), as shown in Table 1. These results indicated that SF-DFO and DFO have identical angiogenesis-promoting potential.

3.3. Bone-seeking effect of SF-deferoxamine

To validate whether there is a bone-seeking effect after combination with IDA, we analyzed the pharmacokinetics of the concentrations of DFO and SF-DFO in the bone tissues of both male and female mice at 0.5, 2, 8, and 24 h after i.v. injection of equal molar masses of the two compounds. The results showed that the concentration of SF-DFO in the femurs and vertebrae remained high, whereas DFO had already been cleared 24 h after i.v. injection (Fig. 4a, b). These results indicated that SF-DFO indeed had a greater bone-seeking propensity compared to DFO.

3.4. Bone microarchitecture and angiogenesis in the metaphysis

Considering the bone-seeking effect of SF-DFO, we assumed that the bone preserving effect would be more efficient in the SF-DFO group than in the DFO group. Equivalent molar masses of the two compounds were injected i.p. every day in OVX mice for 4 weeks, and the trabecular bone microarchitectural parameters in the femurs were analyzed with micro-CT. Three-dimensional reconstruction images of the left distal femurs showed that the trabecular bone was clearly lost in OVX mice, whereas in the SF-DFO group, the trabecular bone was slightly increased relative to that in the DFO and OVX groups (Fig. 5a). Similarly, the micro-CT parameters, including trabecular separation (Tb.Sp) and bone volume per tissue volume (BV/TV), revealed a greater protective effect in the SF-DFO group, although the BMD and trabecular thickness (Tb.Th) were identical between the DFO and SF-DFO groups (Fig. 5b).

To explain the better retention of trabecular mass after SF-DFO treatment, we analyzed the serum collagen type I cross-linked C-telopeptide (CTX-I) and procollagen type I N-terminal propeptide (PINP) levels with ELISA assays, as well as osteoblast and osteoclast number based on histomorphometric analysis. The results showed that the osteoclast number and osteoclast activity were not influenced by DFO and

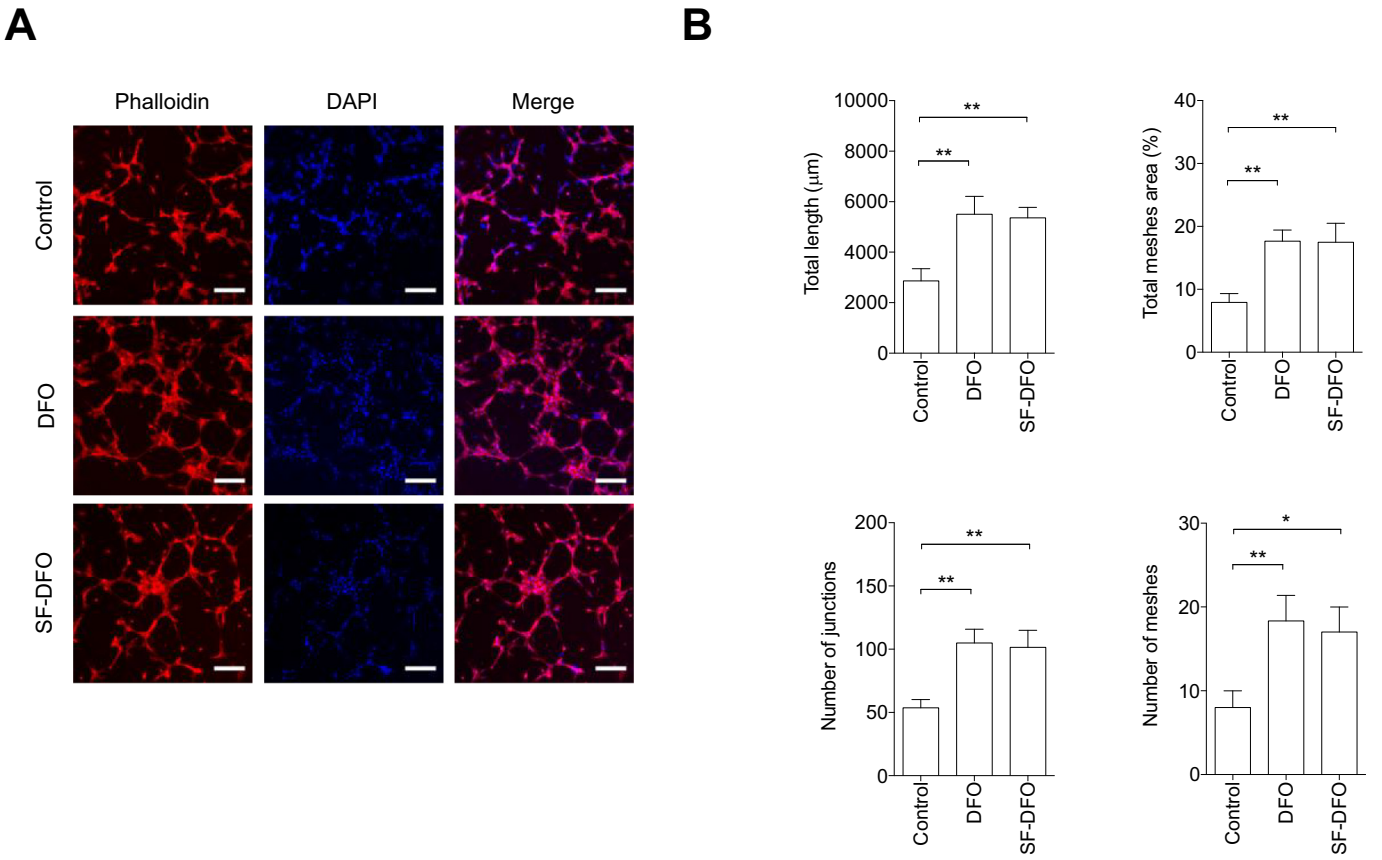

Fig. 3. SF-deferoxamine has an identical angiogenesis-promoting effect to deferoxamine. A) HUVECs cultured in Matrigel were treated with 200 μm SF-DFO or DFO for 12 h. Cellular structures were indicated with Texas red-X conjugated phalloidin staining and DAPI counterstaining. Representative images from three independent experiments are shown. Scale bars, 20 μm. B) Completed tube parameters in five random fields of the images were exported via ImageJ software. One-way ANOVA. Data are represented as the means ± SD. *,P < 0.05. **,P < 0.01.

Table 1
Parameters of complete tube in tube formation assay.

	Total length (μm)	Junction number	Mesh area (%)	Mesh number
Control	2865 ± 480.6	53.7 ± 6.5	7.9 ± 1.4	8.0 ± 2.0
DFO	5500 ± 712.9	105.7 ± 10.8	17.7 ± 1.7	18.3 ± 3.0
SF-DFO	5362 ± 417.8	101.3 ± 13.6	17.5 ± 3.0	17.0 ± 3.0

SF-DFO treatment (Fig. 5c), but the PINP level in the SF-DFO group was increased compared to that in the DFO group, which might have been the result of the increased osteoblast number observed via H&E staining (Fig. 5d).

Next, we analyzed marrow angiogenesis in the femurs. The alpha smooth muscle actin (α-SMA) has relatively restricted expression in vascular smooth muscle cells. Therefore, we performed an α-SMA immunostaining assay and defined the round or elliptical areas surrounded by α-SMA as the blood vessels. Representative images showed that both DFO and SF-DFO inhibited the vascular atrophy induced by OVX and that SF-DFO had a more pronounced effect (Fig. 5e). Quantification of the data regarding the vessel area further demonstrated that angiogenesis after SF-DFO treatment is stronger than that after DFO treatment (Fig. 5f).

3.5. Bone mechanical properties and cortical bone parameters

We also analyzed the microarchitectural parameters of the cortical

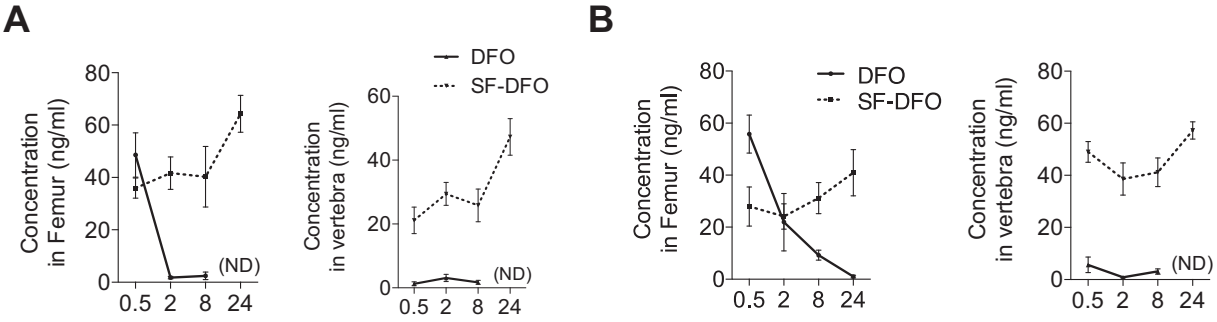

Fig. 4. Bone-seeking effect of SF-deferoxamine. Equal molar masses of SF-DFO or DFO were i.v. injected into mice (n = 3). After 0.5, 2, 8, and 24 h, the muscle-free femurs and vertebrae were isolated and subjected to quantitative measurement with LC-MS/MS. The concentrations of DFO and SF-DFO in female (A) and male (B) mouse tissues were plotted against time separately. One-way ANOVA. Data are represented as the means ± SD. ND, not detected.

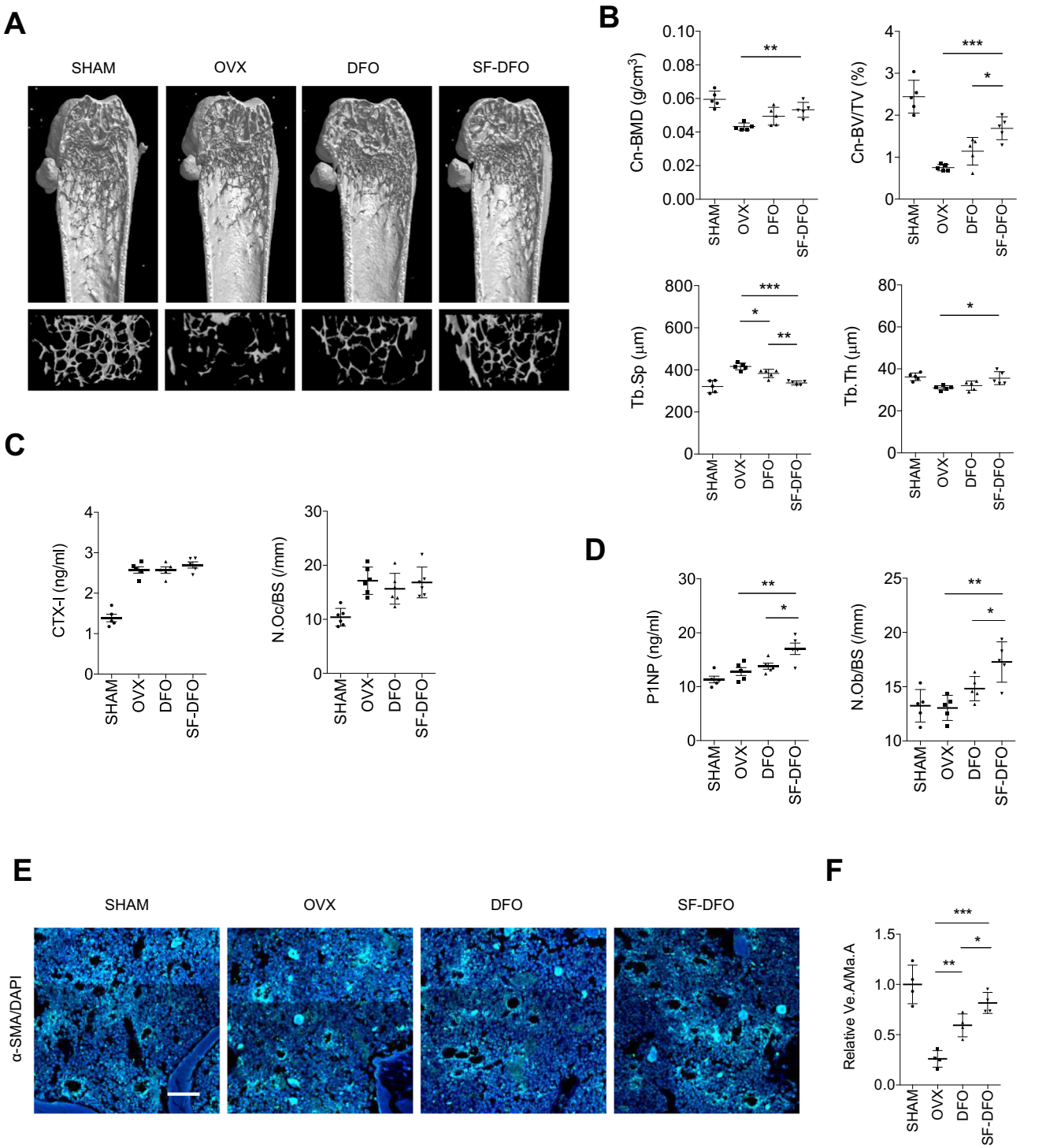

Fig. 5. Bone microarchitecture and angiogenesis in the metaphysis. OVX mice were i.p. injected with DFO and SF-DFO for 4 weeks. A) Left femurs were isolated and subjected to micro-CT analysis. Representative three-dimensional images of distal femurs and relative cross-sections in each group. B) Micro-CT parameters of trabecular bone in cross-sections, including BMD, BV/TV, Tb.Sp and Tb.Th. C) Serum CTX-I level and quantification of osteoclast number per bone surface (N.Oc/BS) in metaphysis. D) Serum PINP level and quantification of osteoblast number per bone surface (N.Ob/BS) in metaphysis. E) Representative images of α-SMA immunostaining in metaphysis. F) Relative ratio of vessel area (α-SMA positive area) to marrow area. Scale bar, 50 μm. n = 5. One-way ANOVA. Data are represented as the means ± SD. *,$P < 0.05$. **,$P < 0.01$. ***,$P < 0.001$.

bone in diaphysis with micro-CT. The results revealed that OVX enlarged the marrow volume (Ma.V) and reduced the cortical thickness (Ct.Th), as well as the porosity (Ct.Po) and tissue mineral density (TMD) of the cortical bone (Fig. 6a, b). In contrast, the DFO and SF-DFO injections reversed these changes in TMD, Ma.V and Ct.Th (Fig. 6a, b).

Furthermore, according to the protective effect of DFO and SF-DFO on the cortical bone, we determined the mechanical properties of the bone tissue after DFO and SF-DFO treatment with a three-point bending test. As expected, OVX led to weaker mechanical properties of the femurs as reflected by lower modulus, ultimate stress, ultimate force, and stiffness, whereas the SF-DFO revealed an identical effect to that of DFO in preventing the OVX-induced loss of bone strength according to these

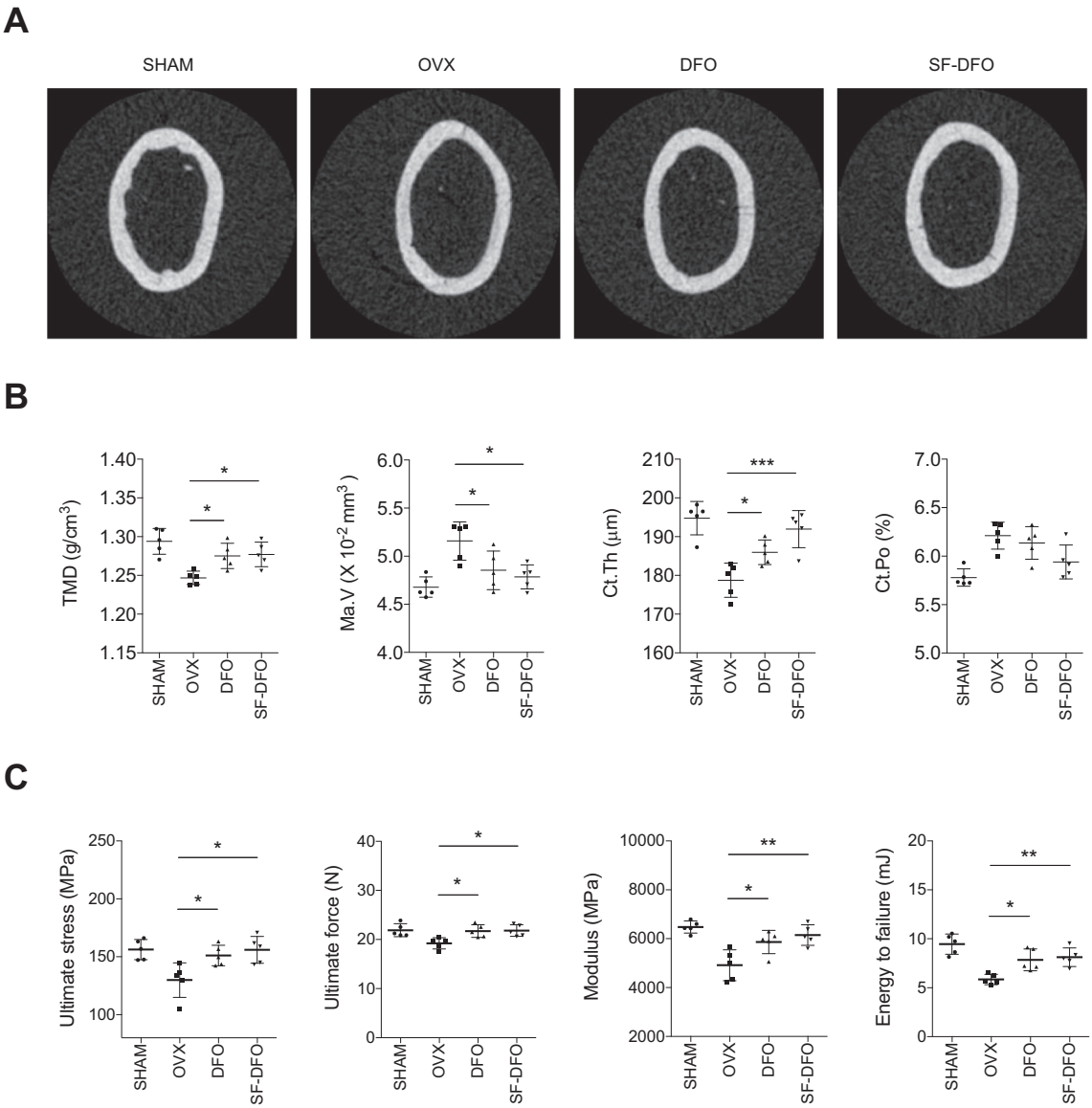

Fig. 6. Bone mechanical properties and cortical bone parameters. OVX mice were i.p. injected with DFO and SF-DFO for 4 weeks. A) Representative images of cortical bone in the diaphysis of the left femurs. B) Micro-CT parameters of cortical bone in cross-sections, including TMD, Ma.V, Ct.Th and Ct.Po. C) Three-point bending parameters of the right femurs, including modulus, ultimate stress, ultimate force and failure energy. n = 5. One-way ANOVA. Data are represented as the means ± SD. *,P < 0.05. **,P < 0.01. ***,P < 0.001.

properties (Fig. 6c).

3.6. Reduced biotoxicity of SF-deferoxamine

To compare the biotoxicities of SF-DFO and DFO, the body weights were recorded every 7 days, and the related organs were all subjected to histopathological examination via H&E staining. The results showed that DFO injection caused continuous weight loss over four weeks, whereas the SF-DFO-treated mice grew normally compared to sham-operation mice (Fig. 7a). Pathologically, DFO caused a diffuse inflammatory response and inflammatory infiltration in the liver and kidney, while SF-DFO did not (Fig. 7b). We also observed granule denaturation, interface hepatitis and piecemeal necrosis of liver cells in the DFO group but not in the SF-DFO group. Furthermore, the germinal center in the white pulp was visible and obviously enlarged in the DFO group, indicating excessive B lymphocyte accumulation. In contrast, all the related organs in the SF-DFO group had no obvious pathological changes based on the histological analysis (Fig. 7b). To further confirm the inflammatory response in related tissues, we detected CD45 (a whole marker of leukocytes)-positive cells using immunohistochemistry. As expected, a large number of CD45-positive cells existed in the liver and splenic red pulp after DFO treatment but not after SF-DFO treatment (Fig. 7c). Thus, SF-DFO was less biotoxic than DFO.

4. Discussion

In the human body, bone tissues are highly vascularized and the blood supply to the ones accounts for approximately 10% of the cardiac output [31]. The causes of postmenopausal osteoporosis include estrogen deficiency [2], as well as a decrease in the number of capillaries in the bone marrow and, therefore, reduced oxygen perfusion [3–5]. In addition, vascular disorders can reduce trabecular bone volume, and the loss of blood supply during surgery leads to a significant decrease in bone density and bone strength [32]. Therefore, vascular degeneration may be one of the mechanisms underlying the pathogenesis of

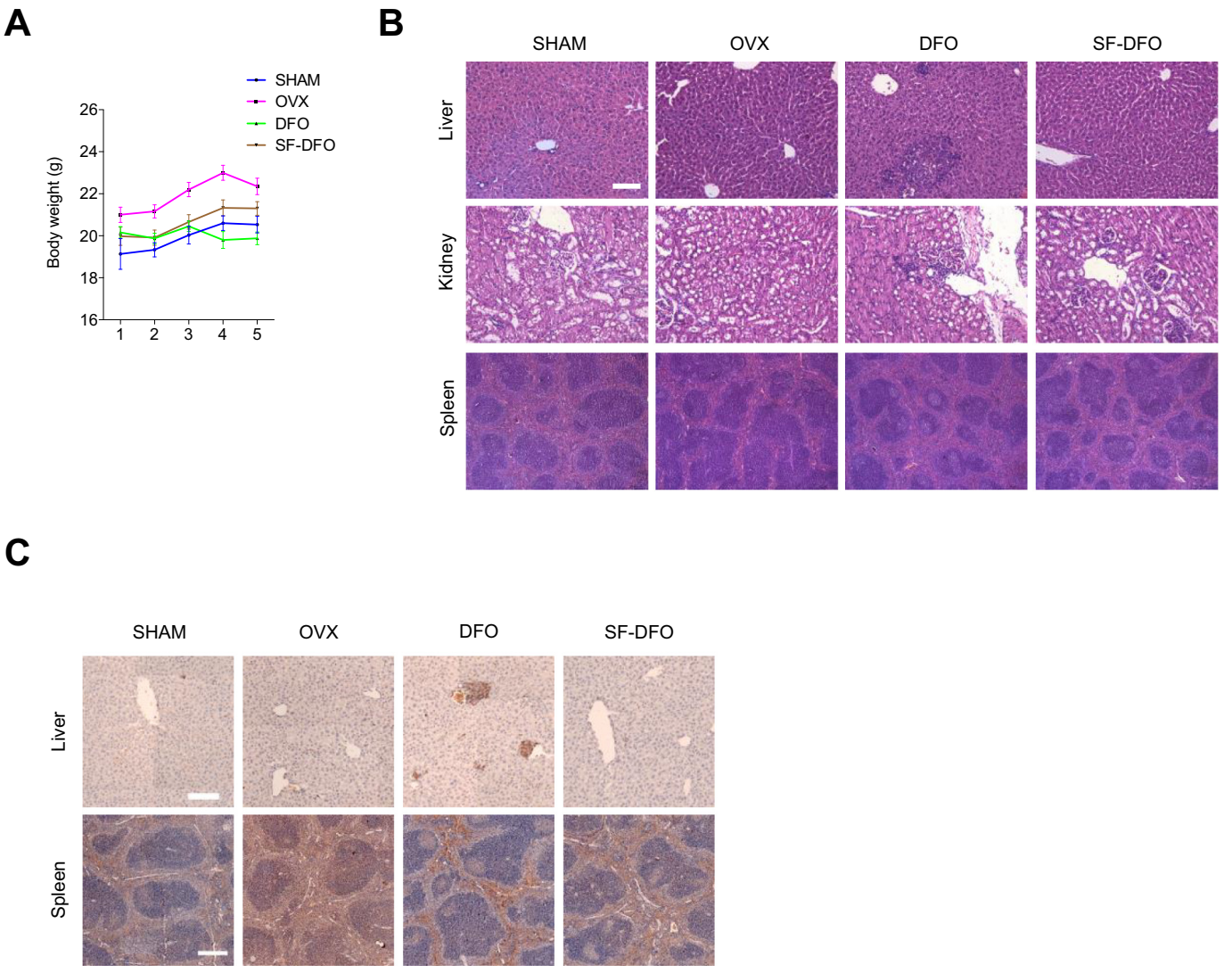

Fig. 7. Reduced biotoxicity of SF-deferoxamine. OVX mice were i.p. injected with the vehicle, DFO or SF-DFO for 4 weeks. A) Body weights were recorded every 7 days and plotted against time (n = 5). B) Representative H&E images of liver, kidney and spleen sections (n = 3). Scale bar, 50 μm. C) Representative CD45 immunohistochemistry images of liver and spleen sections (n = 3). Scale bar: liver, 50 μm, spleen, 200 μm. Data are represented as means ± SD.

osteoporosis.

DFO is a chelating agent that complexes with ferric and trivalent aluminum ions to form complexes but has a low affinity for ferrous (Fe^{2+}), copper (Cu^{2+}), zinc (Zn^{2+}), and calcium (Ca^{2+}) ions. By combining with iron, DFO can reduce the pathological deposition of iron in organs [14]. By chelating the iron required for prolyl hydroxylase, DFO can also activate the HIF-1α pathway, thereby promoting angiogenesis. Our previous study showed that HIFα overexpression in *Vhl*-CKO mature osteoblasts profoundly increased angiogenesis and osteogenesis, which was primarily mediated by VEGF expression [11]. Furthermore, mice with Hif-1α CKO in osteoblasts had decreased bone volume and vascularity [11]. Thus, inducing HIF-1α activation or VEGF expression benefits osteogenesis.

However, the side effects of DFO application have also received increasing attention. First, listening and visual disorders occur during DFO administration. In addition, after oral administration, gastrointestinal irritation may occur; after intramuscular injection, localized pain and sensitization have been reported [20,21]. In our experiment, the i.p. injection of DFO resulted in a diffuse inflammatory response in the spleen, liver and kidney and weight loss, which also clearly indicated the biotoxicity of DFO (Fig. 7).

Bone-seeking molecules are assumed to be capable of binding to calcium or hydroxyapatite, thereby being deposited in bone tissues [33]. By binding with a bone-seeking molecular carrier, osteogenic drugs could have a greater affinity for bone tissues and a lower level of toxicity in other organs. It has been confirmed that tetracycline, bisphosphonate and calcein have a strong affinity for hydroxyapatite [23]. However, there have been many problems in the development of bone-seeking compounds by chemical synthesis, including those involving tetracycline and bisphosphonate. For example, tetracycline modification might attenuate its beneficial activity. Moreover, the complexity and instability of the structure of tetracycline also restricts its usage in chemical synthesis [23,34].

In our previous study, we conjugated estrogen with IDA, a bone affinity molecule, and called the new compound SF-estrogen. SF-estrogen protects bone volume from OVX-induced osteoporosis with few effects on body weight and uterine hypertrophy due to the reduced deposition of drugs in the uterus and the effective accumulation in bone tissue [12]. Thus, we modified DFO with IDA and proved that after covalent modification with IDA, SF-DFO retained the ability to facilitate tube formation by promoting HIF-1α activation and VEGF expression in vitro.

A previous pharmacokinetic study reported that DFO is rapidly cleared from the blood [28]. Our data indicated that DFO stayed in

femurs for only half an hour after the i.v. injection and rapidly cleared within 2 h, whereas the concentration of SF-DFO remained steady for at least 24 h in both femurs and vertebrae, indicating that SF-DFO has excellent bioavailability and stability. Interestingly, the concentration of DFO in the vertebrae appears to be almost negligible within half an hour in both male and female mice relative to the concentrations in the femurs.

For trabecular bone, micro-CT and serum data demonstrated that both DFO and SF-DFO increased the trabecular bone volume via increasing bone formation rather than by reducing bone resorption. However, H&E staining and α-SMA staining revealed that the SF-DFO group had an increased osteoblast number and enriched blood vessels compared to the DFO group. The DFO group always revealed small effects, which, combined with the suboptimal pharmacokinetic performance of DFO, indicates that SF-DFO has a greater protective effect on bone formation than DFO.

In the cortical bone, OVX reduced the cortical thickness, enlarged the marrow volume and increased the porosity in diaphysis, whereas both DFO and SF-DFO attenuated these effects. However, there was no significant difference in bone strength between DFO and SF-DFO, although cortical thickness and porosity were superior in the SF-DFO group.

The newly established compound SF-DFO had low biotoxicity in the related organs. Interestingly, it has been reported that body weight is usually increased after estrogen deficiency [35], and SF-DFO administration obviously attenuated the OVX-induced weight gain.

We would like to note limitations in our study. The mice we used for the OVX model were eight-week-old mice, which still generate new trabecular bone from the growth plate. Thus, the significant differences between groups could be ignored because of low trabecular bone or cortical bone baselines.

In conclusion, by covalently modifying DFO with the bone-affinitive compound IDA, we established a new compound called SF-DFO and proved that SF-DFO retained angiogenesis-promoting capabilities, with lower biotoxicity and a superior effect in preventing OVX-induced trabecular bone loss compared to DFO.

Supplementary data to this article can be found online at https://doi.org/10.1016/j.bone.2018.10.025.

Acknowledgments

We would like to thank Guowei Ni in Shanghai Institute of Pharmaceutical Industry for pharmaceutical technic supports. This work was supported by the National Natural Science Foundation of China (81572099, 81702108, 81700778), Shanghai Science and Technology Commission of Jiading District (JDKW-2017-W10) and Shanghai Municipal Commission of Health and Family Planning (201440411, 20184Y0108).

References

[1] P. Makras, S. Delaroudis, A.D. Anastasilakis, Novel therapies for osteoporosis, Metab. Clin. Exp. 64 (10) (2015) 1199–1214.
[2] F.A. Syed, A.C. Ng, The pathophysiology of the aging skeleton, Curr. Osteoporos. Rep. 8 (4) (2010) 235–240.
[3] T.T. Shih, H.C. Liu, C.J. Chang, S.Y. Wei, L.C. Shen, P.C. Yang, Correlation of MR lumbar spine bone marrow perfusion with bone mineral density in female subjects, Radiology 233 (1) (2004) 121–128.
[4] J.F. Griffith, D.K. Yeung, G.E. Antonio, F.K. Lee, A.W. Hong, S.Y. Wong, E.M. Lau, P.C. Leung, Vertebral bone mineral density, marrow perfusion, and fat content in healthy men and men with osteoporosis: dynamic contrast-enhanced MR imaging and MR spectroscopy, Radiology 236 (3) (2005) 945–951.
[5] Y.X. Wang, J.F. Griffith, A.W. Kwok, J.C. Leung, D.K. Yeung, A.T. Ahuja, P.C. Leung, Reduced bone perfusion in proximal femur of subjects with decreased bone mineral density preferentially affects the femoral neck, Bone 45 (4) (2009) 711–715.
[6] J.H. Min, H. Yang, M. Ivan, F. Gertler, W.G. Kaelin Jr., N.P. Pavletich, Structure of an HIF-1alpha-pVHL complex: hydroxyproline recognition in signaling, Science 296 (5574) (2002) 1886–1889.
[7] B.H. Jiang, J.Z. Zheng, S.W. Leung, R. Roe, G.L. Semenza, Transactivation and inhibitory domains of hypoxia-inducible factor 1alpha. Modulation of transcriptional activity by oxygen tension, J. Biol. Chem. 272 (31) (1997) 19253–19260.
[8] M. Thirunavukkarasu, V. Selvaraju, N.R. Dunna, J.L. Foye, M. Joshi, H. Otani, N. Maulik, Simvastatin treatment inhibits hypoxia inducible factor 1-alpha-(HIF-1alpha)-prolyl-4-hydroxylase 3 (PHD-3) and increases angiogenesis after myocardial infarction in streptozotocin-induced diabetic rat, Int. J. Cardiol. 168 (3) (2013) 2474–2480.
[9] G. He, Y. Jiang, B. Zhang, G. Wu, The effect of HIF-1alpha on glucose metabolism, growth and apoptosis of pancreatic cancerous cells, Asia Pac. J. Clin. Nutr. 23 (1) (2014) 174–180.
[10] J. Myllyharju, P. Koivunen, Hypoxia-inducible factor prolyl 4-hydroxylases: common and specific roles, Biol. Chem. 394 (4) (2013) 435–448.
[11] Y. Wang, C. Wan, L. Deng, X. Liu, X. Cao, S.R. Gilbert, M.L. Bouxsein, M.C. Faugere, R.E. Guldberg, L.C. Gerstenfeld, V.H. Haase, R.S. Johnson, E. Schipani, T.L. Clemens, The hypoxia-inducible factor alpha pathway couples angiogenesis to osteogenesis during skeletal development, J. Clin. Invest. 117 (6) (2007) 1616–1626.
[12] Q. Zhao, X. Shen, W. Zhang, G. Zhu, J. Qi, L. Deng, Mice with increased angiogenesis and osteogenesis due to conditional activation of HIF pathway in osteoblasts are protected from ovariectomy induced bone loss, Bone 50 (3) (2012) 763–770.
[13] D.G. Nagle, Y.D. Zhou, Natural product-derived small molecule activators of hypoxia-inducible factor-1 (HIF-1), Curr. Pharm. Des. 12 (21) (2006) 2673–2688.
[14] G.J. Kontoghiorghes, A. Kolnagou, Deferiprone versus desferrioxamine in thalassaemia, and T2* validation and utility, Lancet 361 (9352) (2003) 184.
[15] G. Lucarelli, R. Clift, E. Angelucci, Deferoxamine in thalassemia major, N. Engl. J. Med. 332 (4) (1995) 271 (author reply 272-273).
[16] X. Shen, C. Wan, G. Ramaswamy, M. Mavalli, Y. Wang, C.L. Duvall, L.F. Deng, R.E. Guldberg, A. Eberhart, T.L. Clemens, S.R. Gilbert, Prolyl hydroxylase inhibitors increase neoangiogenesis and callus formation following femur fracture in mice, J. Orthop. Res. 27 (10) (2009) 1298–1305.
[17] C. Wan, S.R. Gilbert, Y. Wang, X. Cao, X. Shen, G. Ramaswamy, K.A. Jacobsen, Z.S. Alaql, A.W. Eberhardt, L.C. Gerstenfeld, T.A. Einhorn, L. Deng, T.L. Clemens, Activation of the hypoxia-inducible factor-1alpha pathway accelerates bone regeneration, Proc. Natl. Acad. Sci. U. S. A. 105 (2) (2008) 686–691.
[18] G.M. Brittenham, Iron-chelating therapy for transfusional iron overload, N. Engl. J. Med. 364 (2) (2011) 146–156.
[19] Y.L. Chan, C.W. Chu, K.W. Chik, L.M. Pang, M.K. Shing, C.K. Li, Deferoxamine-induced dysplasia of the knee: sonographic features and diagnostic performance compared with magnetic resonance imaging, J. Ultrasound Med. 20 (7) (2001) 723–728.
[20] S.H. Chen, D.C. Liang, H.C. Lin, S.Y. Cheng, L.J. Chen, H.C. Liu, Auditory and visual toxicity during deferoxamine therapy in transfusion-dependent patients, J. Pediatr. Hematol. Oncol. 27 (12) (2005) 651–653.
[21] N.F. Olivieri, J.R. Buncic, E. Chew, T. Gallant, R.V. Harrison, N. Keenan, W. Logan, D. Mitchell, G. Ricci, B. Skarf, et al., Visual and auditory neurotoxicity in patients receiving subcutaneous deferoxamine infusions, N. Engl. J. Med. 314 (14) (1986) 869–873.
[22] A. Cohen, M. Martin, J. Mizanin, D.F. Konkle, E. Schwartz, Vision and hearing during deferoxamine therapy, J. Pediatr. 117 (2 Pt 1) (1990) 326–330.
[23] D. Wang, S.C. Miller, P. Kopeckova, J. Kopecek, Bone-targeting macromolecular therapeutics, Adv. Drug Deliv. Rev. 57 (7) (2005) 1049–1076.
[24] S.C. Miller, H. Pan, D. Wang, B.M. Bowman, P. Kopeckova, J. Kopecek, Feasibility of using a bone-targeted, macromolecular delivery system coupled with prostaglandin E(1) to promote bone formation in aged, estrogen-deficient rats, Pharm. Res. 25 (12) (2008) 2889–2895.
[25] M. Takeyama, K. Nogami, M. Okuda, Y. Sakurai, T. Matsumoto, I. Tanaka, A. Yoshioka, M. Shima, Selective factor VIII and V inactivation by iminodiacetate ion exchange resin through metal ion adsorption, Br. J. Haematol. 142 (6) (2008) 962–970.
[26] Q. Zhao, X. Liu, L. Zhang, X. Shen, J. Qi, J. Wang, N. Qian, L. Deng, Bone selective protective effect of a novel bone-seeking estrogen on trabecular bone in ovariectomized rats, Calcif. Tissue Int. 93 (2) (2013) 172–183.
[27] H. Kang, K. Yang, L. Xiao, L. Guo, C. Guo, Y. Yan, J. Qi, F. Wang, B. Ryffel, C. Li, L. Deng, Osteoblast hypoxia-inducible factor-1alpha pathway activation restrains osteoclastogenesis via the interleukin-33-MicroRNA-34a-Notch1 pathway, Front. Immunol. 8 (2017) 1312.
[28] M.D. Cappellini, K.M. Musallam, A.T. Taher, Overview of iron chelation therapy with desferrioxamine and deferiprone, Hemoglobin 33 (Suppl. 1) (2009) S58–S69.
[29] S. Kumfu, S.C. Chattipakorn, S. Fucharoen, N. Chattipakorn, Effects of iron overload condition on liver toxicity and hepcidin/ferroportin expression in thalassemic mice, Life Sci. 150 (2016) 15–23.
[30] D.W. Dempster, J.E. Compston, M.K. Drezner, F.H. Glorieux, J.A. Kanis, H. Malluche, P.J. Meunier, S.M. Ott, R.R. Recker, A.M. Parfitt, Standardized nomenclature, symbols, and units for bone histomorphometry: a 2012 update of the report of the ASBMR Histomorphometry Nomenclature Committee, J. Bone Miner. Res. 28 (1) (2013) 2–17.
[31] J.H. Park, B.H. Park, H.K. Kim, T.S. Park, H.S. Baek, Hypoxia decreases Runx2/Cbfa1 expression in human osteoblast-like cells, Mol. Cell. Endocrinol. 192 (1–2) (2002) 197–203.
[32] H.P. Gerber, N. Ferrara, Angiogenesis and bone growth, Trends Cardiovasc. Med. 10 (5) (2000) 223–228.
[33] W.M. Pierce Jr., L.C. Waite, Bone-targeted carbonic anhydrase inhibitors: effect of a proinhibitor on bone resorption in vitro, Proc. Soc. Exp. Biol. Med. 186 (1) (1987) 96–102.
[34] F. Bauss, A. Esswein, K. Reiff, G. Sponer, B. Muller-Beckmann, Effect of 17beta-estradiol-bisphosphonate conjugates, potential bone-seeking estrogen pro-drugs, on 17beta-estradiol serum kinetics and bone mass in rats, Calcif. Tissue Int. 59 (3) (1996) 168–173.
[35] J.C. Lin, S. Grampp, T. Link, M. Kothari, D.C. Newitt, D. Felsenberg, S. Majumdar, Fractal analysis of proximal femur radiographs: correlation with biomechanical properties and bone mineral density, Osteoporos. Int. 9 (6) (1999) 516–524.